MODELLING DISCHARGE STIMULATION USING A TRANSIENT WELLBORE SIMULATOR WITH AN AIR-WATER EQUATION OF STATE

Ryan Tonkin[1], John O'Sullivan[1], Michael O'Sullivan[1]

[1]Department of Engineering Science, University of Auckland, Auckland, New Zealand

rton671@aucklanduni.ac.nz

Keywords: *discharge stimulation, air-water EOS, transient, wellbore simulation, gas lifting, air compression.*

ABSTRACT

Simulation of transient flow in geothermal wells is an important reservoir engineering task. Previously, we discussed the development of a wellbore simulator capable of modelling complex transient processes in geothermal wells. However, its applicability was restricted to flows of pure water. This paper discusses the implementation of an air-water equation of state in our transient wellbore simulator. The simulator's capabilities are demonstrated by modelling two discharge stimulation methods, airlifting and air compression. A case study well is considered with a water level approximately 300 m below the wellhead.

1. INTRODUCTION

Transient wellbore simulators are of interest to the geothermal community as they can be used to gain insight into phenomena that are hard to observe. Non-condensable gases such as air and CO_2 can play an important part in wellbore dynamics. Air, for example, often exists at the top of the well when it is shut-in and may be produced in small amounts from the reservoir when a well is opened to flow. Therefore, an air-water equation of state (EOS) is required if some wellbore processes are to be modelled completely (e.g., including opening and closing of the well).

Transient geothermal wellbore simulators have been developed by Miller (1980), García-Valladares (2006), Pan et al. (2011) and Akbar et al. (2016). Of these simulators, T2WELL by Pan et al. (2011) is the only one capable of modelling flows of a mixture of water and non-condensable gases. T2WELL was first used with the ECO2N EOS to model carbon sequestration problems. Although T2WELL was initially designed for low-temperature fluids with high CO_2 content, it has since been extended to encompass higher temperature fluids using the ECO2H EOS (Pan et al., 2015). T2WELL has also been used in geothermal applications by Vasini et al. (2018) with the EWASG EOS, which accounts for CO_2 and NaCl, to model production tests from a slim well in the Wotton Waven Field. More recently, Battistelli et al. (2020) coupled T2WELL to EOS2H to model the flow of supercritical mixtures of CO_2 and water. They modelled output curves for the IDDP-1 well in the Krafla geothermal field, Iceland.

Previously, we presented a transient simulator capable of modelling complex flows of pure water in geothermal wells (Tonkin et al., 2020). Our simulator uses a fully implicit numerical implementation with hybrid upstream weighting. Additionally, the drift flux constitutive model, which describes phase slip, is solved implicitly at the same time as the conservation equations. The present work discusses the extension of this transient geothermal wellbore simulator so that it can handle the flow of mixtures of water and air. Section 2.1 presents the conservation equations that govern the flow of air-water mixtures in a geothermal wellbore. The governing equations are solved numerically using total pressure, temperature (switched with saturation for two-phase flow), vapour velocity, liquid volume flux and the partial pressure of air as primary variables. Section 2.2 discusses how the secondary variables (i.e., the properties of each phase) are calculated from these primary variables.

Air can be used to stimulate wells that will not flow on their own, which is referred to as discharge stimulation. Wells can be stimulated by the injection of air in two ways: firstly, by pumping air into the top of a well, building up pressure and then releasing it (referred to as air compression) or, secondly, by pumping gas, in our case air, into the bottom of a well (referred to as gas lifting). We model discharge stimulation using these methods on a case study geothermal well to demonstrate the ability of our simulator to model the complex flow of air-water mixtures. These simulations are presented in Section 3.

2. AIR-WATER MODEL FOR GEOTHERMAL WELLS

Transient flow in geothermal wells is modelled by considering the conservation of mass, momentum and energy. Mass conservation equations are given for both the air and water components in (1) and (2). Equations (4) and (5) describe the conservation of momentum and energy for the air-water mixture. Section 2.2 defines the phase variables, density and enthalpy, for example, for air-water mixtures. The other constitutive models used in this simulator require no modifications with the inclusion of air and are discussed elsewhere (Tonkin et al., 2020).

2.1 Conservation equations with air

The conservation of mass for the air component is:

$$\frac{\partial}{\partial t}[\rho_l S_l x_l^a + \rho_v S_v x_v^a] + \frac{1}{A}\frac{\partial}{\partial s}[A\rho_l S_l u_l x_l^a + A\rho_v S_v u_v x_v^a] - q_{mass}^a = 0. \quad (1)$$

Similarly, the mass conservation equation for the water component is:

$$\frac{\partial}{\partial t}[\rho_l S_l x_l^w + \rho_v S_v x_v^w] + \frac{1}{A}\frac{\partial}{\partial s}[A\rho_l S_l u_l x_l^w + A\rho_v S_v u_v x_v^w] - q_{mass}^w = 0. \quad (2)$$

ISSN 2703-4275

In (1) and (2), the mass fraction of component κ in phase β is represented by x_β^κ, defined as:

$$x_\beta^\kappa = \frac{M_\beta^\kappa}{M_\beta}, \tag{3}$$

where M_β^κ is the mass of component κ in phase β and M_β is the total mass of phase β. It follows from (3) that $x_\beta^a + x_\beta^w = 1$.

In (1) and (2), ρ_l and ρ_v are the densities of the liquid and vapour phases. They are the mass-averaged density of the air and water components and are defined in (6) and (14) below for the liquid and vapour phases, respectively. The saturation and average velocity of phase β are given by S_β and u_β, respectively. We assume that the dissolved air flows at the same velocity as the liquid phase, while gaseous air and water vapour have the same average velocity. Finally, the mass exchange between the reservoir and the wellbore for a component κ is given by $q_{mass}^\kappa = x_f^\kappa q_{mass}$. Here, x_f^κ is the flowing mass fraction of component κ for the feed and q_{mass} is the total mass source term, which is defined elsewhere (Tonkin et al. 2020).

The conservation of momentum for a two-phase mixture is:

$$\frac{\partial}{\partial t}[\rho_l S_l u_l + \rho_v S_v u_v] + \frac{1}{A}\frac{\partial}{\partial s}[A\rho_l S_l u_l^2 + A\rho_v S_v u_v^2] + \frac{\partial P}{\partial s} + \frac{2}{r}\tau + (\rho_l S_l + \rho_v S_v) g \frac{\partial z}{\partial s} - q_{mom} = 0. \tag{4}$$

Here, P is pressure, $g = 9.81$ m/s^2 is gravitational acceleration, z is vertical depth, and s is the distance along the wellbore. The wellbore radius is given by r, while A denotes the cross-sectional area of the wellbore, and q_{mom} is the external momentum source or sink term. Wellbore friction, τ, is defined by a constitutive model discussed elsewhere (Tonkin et al., 2020).

The conservation of energy for a two-phase mixture is:

$$\begin{aligned}&\frac{\partial}{\partial t}\left[\rho_l S_l \left(h_l + \frac{u_l^2}{2}\right) + \rho_v S_v \left(h_v + \frac{u_v^2}{2}\right) - P\right] \\ &\quad + \frac{1}{A}\frac{\partial}{\partial s}\left[A\rho_l S_l u_l \left(h_l + \frac{u_l^2}{2}\right) + A\rho_v S_v u_v \left(h_v + \frac{u_v^2}{2}\right)\right] + (\rho_l S_l u_l + \rho_v S_v u_v) g \frac{\partial z}{\partial s} + q_{heat} - q_{ener} = 0.\end{aligned} \tag{5}$$

Here, h_l and h_v are the enthalpies of the liquid and vapour phases. They are the mass-averaged enthalpy of the air and water components and are defined in (10) and (17) for the liquid and vapour phases, respectively. Finally, q_{heat} models heat transfer between the wellbore and the surrounding reservoir and q_{ener} models energy transfer due to fluid exchange with the reservoir.

2.2 Air-water equation of state

The governing conservation equations and an additional equation governing phase slip by Shi et al. (2005) are solved implicitly for five primary variables. We found that pressure, temperature (swapped with saturation for two-phase conditions), vapour velocity and liquid volume flux provided the best numerical performance for our simulator when modelling pure water. The partial pressure of air, persistent across all phase states, is chosen as the fifth primary variable. The calculation of secondary variables from these primary variables is presented in Sections 2.2.1 and 2.2.2 for the liquid and vapour phases. It is similar to the method used in the geothermal reservoir simulator Waiwera (Croucher, 2020).

2.2.1 Liquid phase

The effect of dissolved air on the liquid density and viscosity, ρ_l and μ_l, is assumed to be negligible, therefore:

$$\rho_l = \rho_l^w; \tag{6}$$

$$\mu_l = \mu_l^w. \tag{7}$$

Here, ρ_l^w and μ_l^w are the density and viscosity of liquid water, which are calculated using the IAPWS97 thermodynamic equations as functions of the partial pressure of water, P^w, and temperature, T (Dittmann, 2000). The partial pressure of water is known from:

$$P^w = P - P^a. \tag{8}$$

Here, the total pressure, P, and the partial pressure of air, P^a, are calculated as primary variables regardless of the fluid phase state. The physical meaning of P^a is somewhat different under single-phase liquid conditions, where it corresponds to the pressure required to keep all the air in solution.

Temperature is used as a primary variable for single-phase flow. When two-phase conditions exist, the temperature of the fluid mixture is the saturation temperature, T_{sat}, of the water phase calculated using the IAPWS97 formulation:

$$T = T_{sat}(P^w). \tag{9}$$

Calculation of the liquid enthalpy must take air into account. It is calculated using the component mass fractions:

$$h_l = x_l^w h_l^w + x_l^a (h_l^a + h_{sol}^a), \tag{10}$$

where, h_l^w is the enthalpy of liquid water, h_l^a is the enthalpy of air in the liquid phase and h_{sol}^a is the heat of solution. For air, the heat of solution is assumed to be zero. Essentially the same method discussed here for water-air mixtures can be used for water-CO_2 mixtures, where for CO_2, the heat of solution is not zero.

ISSN 2703-4275

The mass fractions for the liquid phase are calculated using Henry's law. First, the mole fraction is calculated:

$$m_l^a = \frac{P^a}{k_h}, \tag{11}$$

where P^a is the partial pressure of air and Henry's Coefficient, k_h, is assumed to have a constant value of 10^{10}. Then the mass fraction of air in the liquid phase is calculated from the mole fraction using the molecular weights of air and water, MW^a and MW^w:

$$x_l^a = \frac{m_l^a MW^a}{m_l^a MW^a + (1 - m_l^a) MW^w}. \tag{12}$$

Finally, the mass fraction of water in the liquid phase is calculated as:

$$x_l^w = 1 - x_l^a. \tag{13}$$

2.2.2 Vapour phase

We calculate the average vapour density using Dalton's law:

$$\rho_v = \rho_v^w + \rho_v^a, \tag{14}$$

where the water vapour density, ρ_v^w, is calculated using the IAPWS97 equations as a function of P^w and T, and the air density, ρ_v^a, is calculated using the ideal gas law as a function of P^a and T. Again, the temperature is known as a primary variable for single-phase flow and from (9) when two-phase conditions exist.

The mass fraction of air in the vapour phase is calculated as the ratio of air density to total density:

$$x_v^a = \frac{\rho_v^a}{\rho_v^w + \rho_v^a}. \tag{15}$$

After calculating (15), the mass fraction of water in the vapour phase is calculated as:

$$x_v^w = 1 - x_v^a. \tag{16}$$

The average vapour enthalpy is calculated from the mass fractions:

$$h_v = x_v^w h_v^w + x_v^a h_v^a. \tag{17}$$

Here, h_v^w is the enthalpy of water vapour and h_v^a is the enthalpy of air. The enthalpy of water vapour is calculated as a function of P^a and T using the IAPWS97 relationships for pure water (Dittmann, 2000). The enthalpy of air is calculated based on the formula from (Irvine and Liley, 1984), shifted to equal zero at the triple point of water, as a function of T. Finally, the viscosity of the air-water vapour mixture, μ_v, is calculated in the same way as in the geothermal reservoir simulator Waiwera, which uses an equation by Hirschfelder et al. (1954), modified to improve the empirical model for vapour viscosity.

3. MODELLING DISCHARGE STIMULATION IN GEOTHERMAL WELLS

Many geothermal wells are self-discharging, meaning that flow is initiated by first shutting the well, allowing it to heat up and build pressure, then simply opening the wellhead to flow. However, non-self-discharging wells fail to build sufficient pressure after shut-in. Instead, the top section of the well is filled with cold air, and the water level may be hundreds of metres below the wellhead. These non-self-discharging wells can occur in conventional liquid dominated geothermal systems and have been reported in Indonesia, the Philippines, Costa Rica, Iceland, Iran, Mexico, Kenya and New Zealand (Mubarok and Zarrouk, 2017). The inability of a well to flow can be caused by a combination of several factors, including (Mubarok and Zarrouk, 2017):

- Deep natural water levels, e.g., due to high elevation terrain
- Slow temperature recovery after well testing
- Cold temperatures in shallow formations
- Damage to the well during drilling
- Low reservoir permeability
- Significant pressure or temperature decline in the reservoir

If a well will not self-discharge for any of the reasons listed above, then flow may be brought about by stimulation. Two methods of discharge stimulation are gas lifting and air compression. The cost of a typical air compression program is approximately 50,000 USD. In comparison, gas lift programs, which are typically seen as a last resort when other stimulation methods do not work, can cost anywhere between 150,000 – 500,000 USD per well, depending on the cost of mobilising a coiled tubing unit (Mubarok and Zarrouk, 2017). Given the high cost of these methods, numerical simulation can provide low-cost insight to aid decision making.

Numerical simulation of air compression and airlifting processes requires a transient wellbore simulator with air-water capabilities to: 1) model the air cap in the top section of the shut-in well, and 2) model the injection of air at either the wellhead or at depth to stimulate flow. Section 3.1 presents the stationary conditions that are used as initial conditions. Discharge stimulation using airlifting and air compression are then discussed in Sections 3.2 and 3.3, respectively. The same wellbore is used for both simulations, and its properties are given in Tables 1 and 2. Here, α is a lumped parameter describing the productivity of the feed (Tonkin et al. 2020).

ISSN 2703-4275

Table 1: Parameters and locations of reservoir and atmospheric feed zones for the simulation of initial conditions.

Name	Elevation [mRL]	P [bara]	h_{fmix} [kJ/kg]	α [kg/s/Pa]	x_f^a [-]
Reservoir	-990 to -1000	60	1085	3E-6	0
Atmospheric feed	0 to -10	1.01325	25	3E-6	0.9999

Table 2: Wellbore and simulation parameters for all simulations.

Length	1000 m
Inclination	0°
Diameter	0.2 m
Completion diameter	0.3 m
Discretisation	Uniform, 100 elements
Heat flux model	Analytical: Ramey (1962)
Slip model	Drift-flux model by Shi et al. (2005)
Overall heat transfer coefficient	35 W/m^2/K
Feed-zones properties	Table 1
Pipe roughness	4.5E-5 m
Bottomhole boundary	Closed
Formation temperature	Figure 1 B)

3.1 Simulating realistic initial conditions

When shut-in, non-self-discharging wells have a water level below the wellhead. These are the conditions that have to be used as initial conditions when modelling wellbore stimulation procedures. Below we describe the process of how we obtain realistic initial conditions for the case study well through simulation.

We use a 1000 m vertical well with a constant diameter of 0.2 m to demonstrate the simulation of discharge stimulation. Additional wellbore and simulation properties are given in Table 2. The reservoir is modelled using a single feed, whose properties are given in Table 1, located at the bottom of the well. These feed properties correspond to liquid water at approximately 60 bara and 250 °C. The formation temperature profile corresponding to a liquid dominated system is used in these simulations and is constant with time. Here, the top 300 m has a linear temperature transition from 25–100 °C. Below -300 mRL, it is the boiling point temperature profile with a maximum temperature of 250 °C. A second source term, which we call the "atmospheric feed", controls the inflow and outflow of air through the wellhead. Its properties, given in Table 1, correspond to 25 °C air at sea level, and its use is discussed further below.

A well is typically shut-in by first injecting cold water to suppress up-flow, then closing the wellhead. If the water level begins to drop after shut-in, the wellhead pressure will drop below atmospheric conditions. If this occurs, the wellhead is opened slightly, allowing a small amount of air into the well. This allows the wellhead pressure to return to atmospheric conditions and for the water level to drop. We represent this process in our simulation using a one-way "atmospheric feed" prescribed in the top block of the wellbore model. This feed models the wellhead control processes by allowing air to be drawn into the well but prevents outflow. Modelling the inflow of air in this way requires the productivity of the atmospheric feed to be specified. We chose this arbitrarily to be the same as the reservoir productivity. Note that because this feed is prescribed in the top block of the wellbore model, it is located slightly below the surface.

To simulate this process, we first inject liquid water at 25 °C, then shut the wellhead for a period of 30 days. After shut-in, the hydrostatic pressure of the liquid column in the well is greater than the reservoir feed-zone pressure. As a result, wellbore fluid flows out into the feed. This reduces the pressure in the wellhead block slightly, so that it is below the pressure of the atmospheric feed. This activates the feed and draws air into the well. The water level continues to drop until equilibrium conditions are reached, which occur when the net mass flow into the well is zero.

If boiling occurs at any point during the heat-up process, the one-way atmospheric feed prevents outflow and allows the pressure in the well to increase. If significant boiling were to occur, the associated increase in pressure might be sufficient to enable the well to flow on its own without needing stimulation. Simulating the wellhead conditions in this way allows us to predict whether a well is likely to self-discharge or whether it will require stimulation. Figure 1 shows that, for this case, the well has failed to build up sufficient pressure after 30 days. In fact, the wellhead pressure increases to 1.4 bara due to a small amount of boiling, and the shut-in water level is approximately 275 m below the wellhead. This is shown by the change in pressure gradient in Figure 1 A) and the rapid increase in vapour saturation in Figure 1 C). This well will require stimulation because of its low wellhead pressure and deep water level. We discuss the simulation of discharge stimulation using gas lifting and air compression below.

3.2 Modelling discharge stimulation: gas lifting

Gas lifting involves pumping a compressed gas to some depth below the water level in the well using a coiled tubing unit. While air has been used in past gas lifting operations, nitrogen is a more common choice of gas because it is chemically stable and non-corrosive (Mubarok and Zarrouk, 2017). However, as air is approximately 80% nitrogen, the density, solubility, and heat capacity of the two gases are similar, meaning air-water simulations can be used to gain valuable insight into gas lifting in geothermal wells.

ISSN 2703-4275

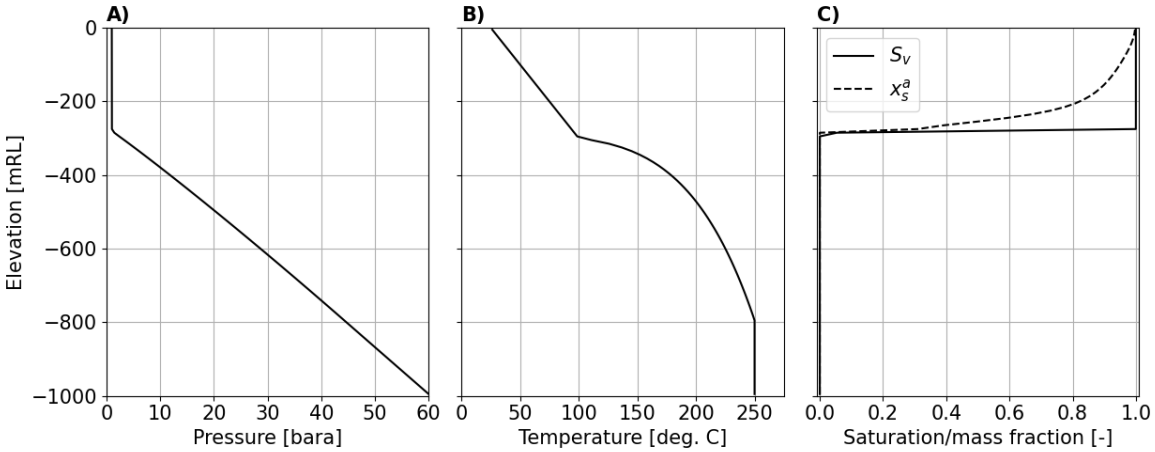

Figure 1: Initial conditions for A) pressure, B) temperature, and C) vapour saturation and air mass fraction for a well with a water level below the wellhead after the process described in Section 3.1.

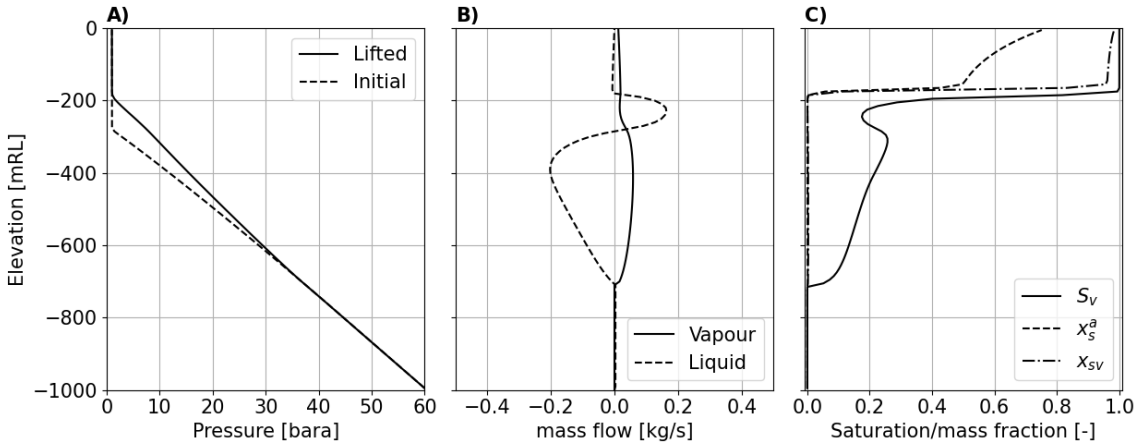

Figure 2: Conditions after 30 minutes of airlifting at 0.01 kg/s for A) pressure, B) phase mass flows, and C) vapour saturation, S_v, static vapour mass fraction, $x_{sv} = M_v/M$, and static air mass fraction, $x_s^a = M^a/M$, for the well in Section 3.1.

The airlifting of a geothermal well has been simulated by Akbar et al. (2016), however, their simulation did not explicitly model air. Instead, the entire wellbore was initialised with an approximate air-water mixture with a modified density and heat capacity. We present a more physically accurate simulation of airlifting, which starts from the realistic static conditions given in Figure 1. Air was injected at a depth of 705 m, approximately 425 m below the water level, at different mass flow rates until sustainable flow was achieved. In Section 3.2.1, we discuss injection at a mass flow rate of 0.01 kg/s, which failed to stimulate the well. In Section 3.2.2, we discuss how sustained discharge is achieved by increasing the mass flow rate to 0.05 kg/s.

3.2.1 Failed lift

Initially, air was injected at a mass flow rate of 0.01 kg/s for 30 minutes. It was found that this rate, depth and time period of injection was insufficient to raise the water level to the wellhead and stimulate discharge. Instead, Figure 2 A), which compares the initial pressure to the pressure at 30 minutes, shows that the water level was only lifted by approximately 100 m. This lift failed because, at this injection rate, the velocity of the air rising through the liquid is not large enough to entrain the water and prevent down-flow in the liquid phase. This down-flow is shown in Figure 2 B) which plots the phase mass flows.

The injected air, which has mixed with a small amount of water vapour, rises slowly from the top of the liquid column. As the air-water vapour mixture flows towards the wellhead, it loses energy to the cooler formation. This causes some of the water vapour to condense, which is shown in Figure 2 C) by the increase in air mass fraction from 50% to 75% between the water level and the wellhead. This results in a small down-flow of liquid condensate in the top 200 m of the well, which is shown in Figure 2 B).

3.2.2 Successful lift

The well was successfully discharged by increasing the rate of air injection to 0.05 kg/s. The results of this simulation are shown in Figure 3. Note that the drop in temperature at -700 mRL in Figure 3 B) is caused by injecting cold air at 25 °C.

Figure 3 C) shows (in black) that three minutes of injection at the increased rate of 0.05 kg/s has caused up-flow above -700 mRL. At this increased flow rate, the velocity of the vapour phase is large enough to begin dragging the liquid up the well. Additionally, the expansion of the gas as it progresses up the well displaces the water above it.

ISSN 2703-4275

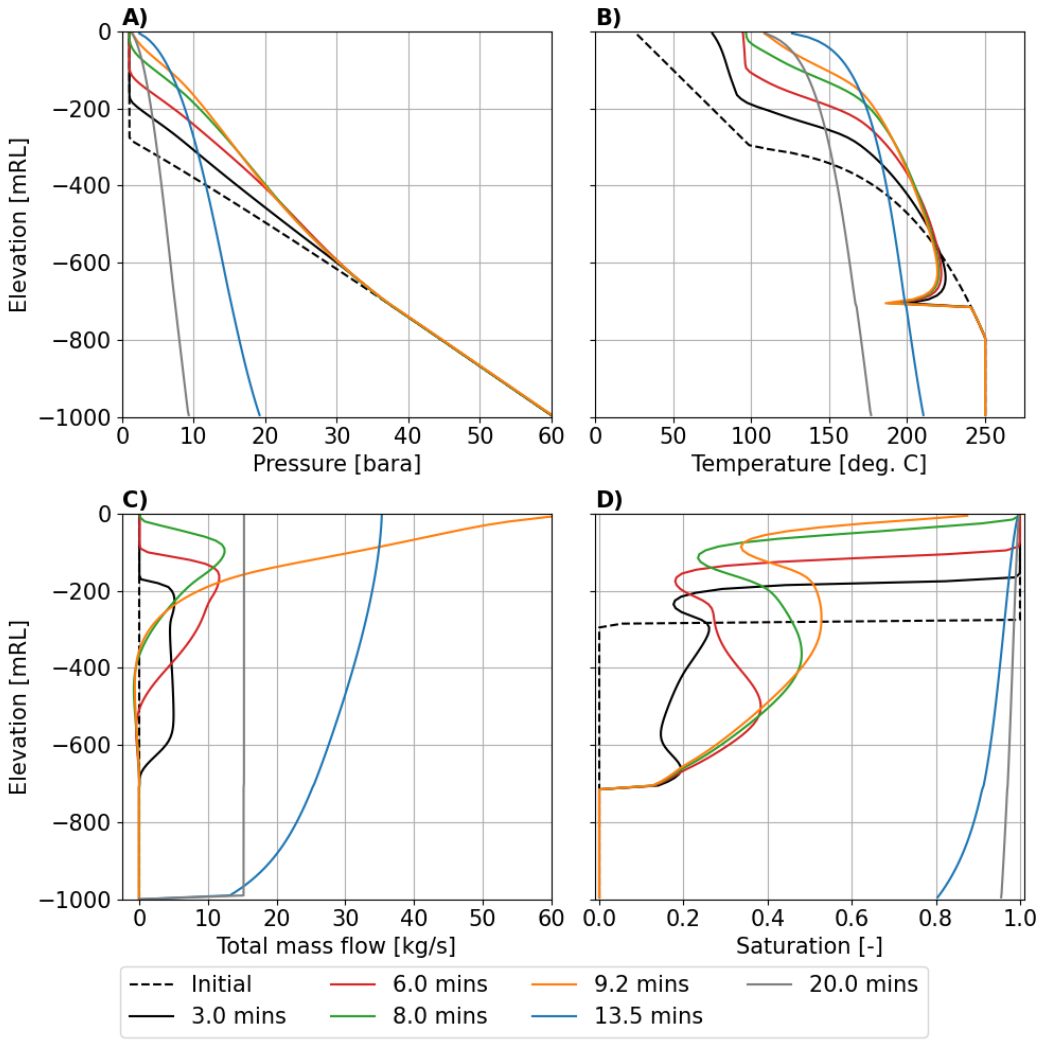

Figure 3: Results of successful airlifting with an air mass flow rate of 0.05 kg/s showing A) pressure, B) temperature, C) total mass flow and D) vapour saturation at various times for the well described in Section 3.1.

After approximately 9 minutes of injection, the water level reaches the wellhead, as shown by the pressure profiles in Figure 3 A) and the drop in wellhead saturation in Figure 3 D) (shown in orange). Shortly after this time, sufficient heat has been transported up the well for flashing to begin at the wellhead. This causes a significant increase in mass flow at the wellhead shown in Figure 3 C) (similarly in orange). This flashing is required for the wellbore to flow without additional air injection. Pressures drop rapidly as flashing progresses down the well. Figure 3 A) shows (in blue) that after 13.5 minutes of injection, approximately 4 minutes after the onset of flashing, the bottomhole pressure has dropped below 20 bara, and hot geothermal fluid is produced at 12kg/s from the feed zone. After 20 minutes, the well has reached stable conditions and no longer requires stimulation.

3.3 Modelling discharge stimulation: air compression

During air compression, air is injected at the wellhead to depress the water level and force fluid into the reservoir. After allowing the cold fluid to be heated by the reservoir, the wellhead is opened to flow. The rapid drop in wellbore pressures causes production from the feed-zone and an influx of hot fluid. Flashing induced in the well by the in-flowing fluid is hopefully sufficient to sustain low hydrostatic pressures and continue production. The wellhead pressure required to stimulate flow varies depending on the feed properties and the length and temperature of the fluid column. We model air compression using two separate simulations. The first simulation models the compression of the liquid column, and the second simulates opening the well to flow. The simulations are discussed in Sections 3.3.1 and 3.3.2, and results are shown in Figures 4 and 5, respectively.

3.3.1 Compression simulation

The compression simulation starts from the stable initial conditions given in Figure 1 above. Air is injected at the wellhead at a fixed rate of 0.05 kg/s for 5 hours using a source term in the top block of the wellbore model. Injecting air increases the wellhead pressure, which increases bottom-hole pressure, forcing fluid into the reservoir feed zone and lowering the water level. After compression, Figure 4 A) shows the wellhead pressure has risen to approximately 27 bara, and Figure 4 C) shows the water level has dropped 300 m to a depth of 600 m. The well remains shut-in for 24 h to allow time for it to heat up.

ISSN 2703-4275

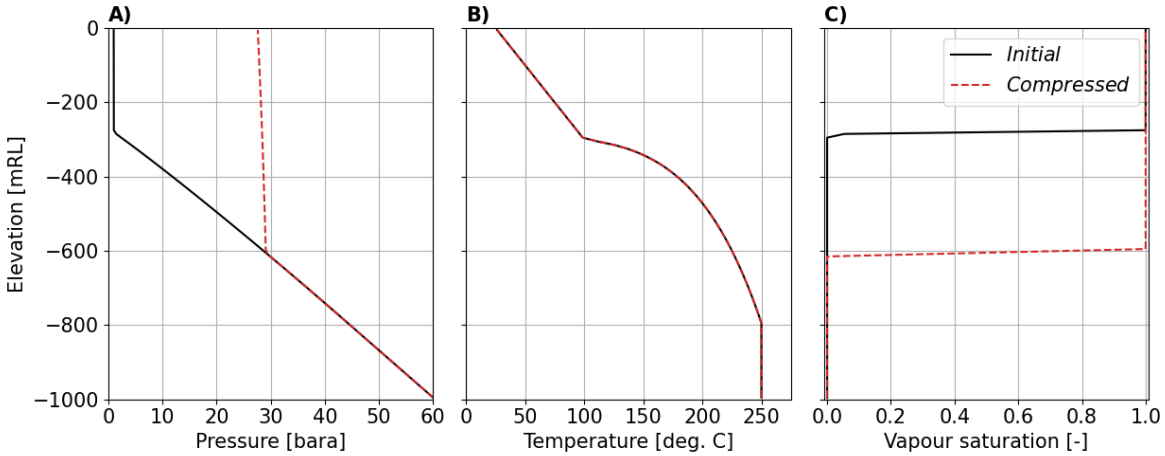

Figure 4: A) Pressure, B) temperature, and C) vapour saturation profiles before and after air compression at 0.05 kg/s for five hours for the well described in Section 3.1.

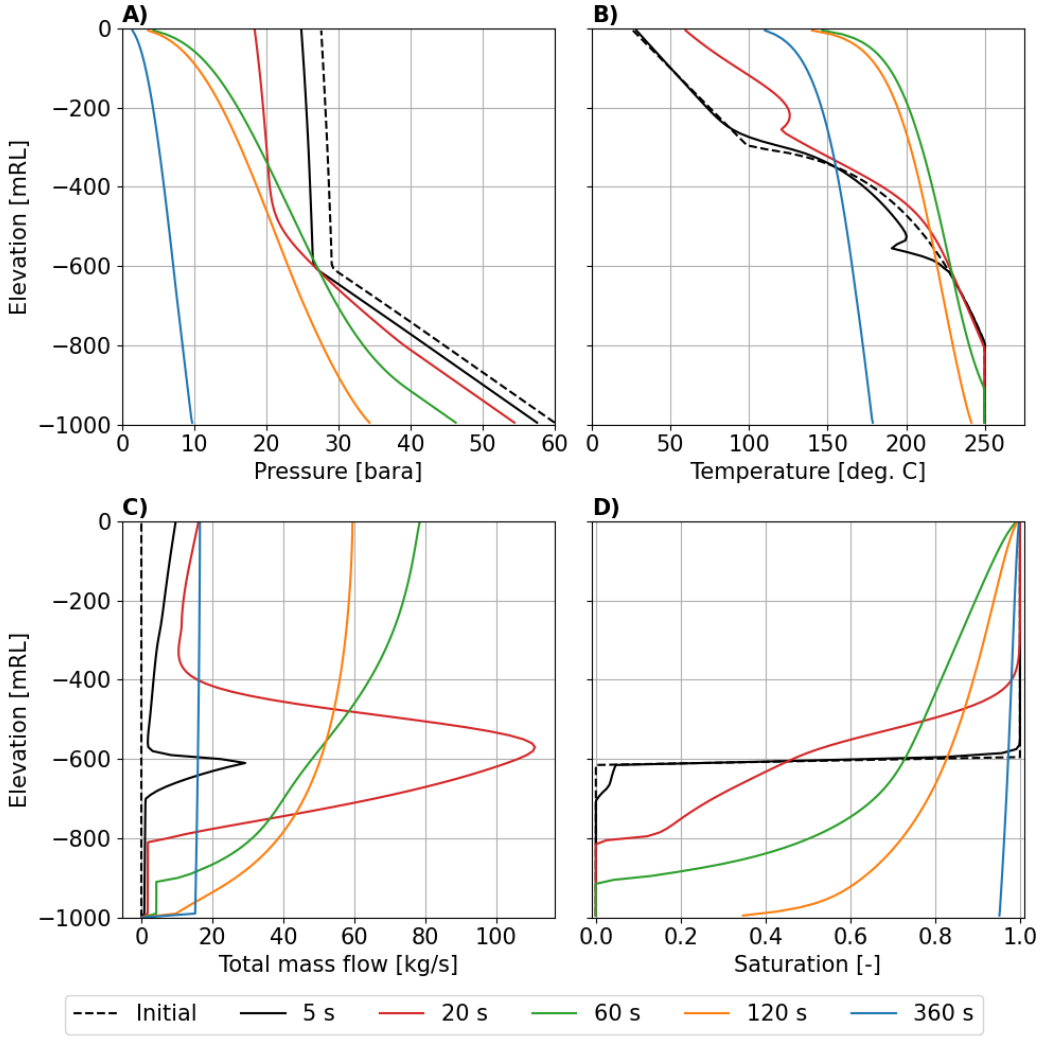

Figure 5: Results of discharge stimulation with a compressed pressure of 27 bara showing A) pressure, B) temperature, C) total mass flow and D) vapour saturation at various times after opening the well described in Section 3.1.

3.3.2 Depressurisation simulation

Wellbore flow is initiated by dropping the wellhead pressure from the compressed value of 27 bara to atmospheric conditions (1.01325 bara) linearly over 60 seconds. Figure 5 A) shows that reducing the wellhead pressure causes the pressure to drop at all depths. Figure 5 D), which shows vapour saturation, indicates that this pressure drop initiated a rapid flashing process almost immediately at the air-water interface. This is because the liquid at this depth is at 225 °C and has a saturation pressure of approximately 25 bara (only 2 -

ISSN 2703-4275

3 bar below the compressed pressure). The onset of rapid flashing causes fluid expansion and the acceleration of the two-phase fluid up the well, as shown by the large increase in mass flow in Figure 5 C). During this process, over 60 seconds, the wellhead temperature increases from 25 °C to 150 °C. This rapid heating would place considerable thermal stress on the well. Figure 5 D) shows that the entire well has flashed after two minutes, which decreases the bottomhole pressure further, causing overpressure in the feed and the production of hot geothermal fluid. After six minutes, the feed produces fluid at approximately 15 kg/s, and the wellbore flow has stabilised.

4. CONCLUSIONS

This paper outlines the extension of the capability of our transient geothermal wellbore simulator to model flows of air-water mixtures. We outlined the conservation equations for air-water mixtures and the procedure for calculating the thermodynamic parameters of each phase. We then demonstrated the ability of our simulator to model the complex flow of air-water mixtures by simulating discharge stimulation methods for a sample well. The well was successfully discharged using gas lifting (with air) and air compression starting from realistic initial conditions. For this well, it was found that injecting 0.01 kg/s of air at a depth of 705 m was insufficient to induce wellbore flow. Increasing the mass flow to 0.05 kg/s successfully lifted the water level to the height of the wellhead and induced flow. When using air compression, it was found that a wellhead pressure of 27 bara was sufficient to induce flashing and cause the well to flow.

The case study presented in this work was relatively simple and designed to showcase the simulation of stimulation methods using air. In many cases, wellbore temperatures are significantly lower than in our example, meaning hot geothermal fluid must be produced from the reservoir before flashing will occur. This leads to more prolonged and more difficult stimulation procedures. Internal circulation between feeds can have a similar effect. These effects can be so pronounced that, in some cases, air compression will not induce flow and stimulation using gas lifting can be difficult. We have demonstrated here and elsewhere that our transient simulator can model complex phenomena such as counter-flow, inter-zonal flow and rapid flashing in a well. This makes it a useful tool to aid decision making for these more difficult stimulation procedures as well as other complex air-water scenarios.

REFERENCES

Akbar, S., Fathianpour, N. and Al-Khoury, R.: A Finite Element Model for High Enthalpy Two-Phase Flow in Geothermal Wellbores, *Renewable Energy* **94**, 223–236. (2016).

Battistelli, A., Finsterle, S., Marcolini, M. and Pan, L.: Modeling of Coupled Wellbore-Reservoir Flow in Steam-Like Supercritical Geothermal Systems, *Geothermics* **86**. (2020).

Croucher, A.: Waiwera User Guide, Technical Report. (2020).

Dittmann, A.: IAPWS Industrial Formulation 1997 for the Thermodynamic Properties of Water and Steam, *International Steam Tables* **122**, 7–150. (2000).

García-Valladares, O., Sánchez-Upton, P. and Santoyo, E.: Numerical Modeling of Flow Processes Inside Geothermal Wells: An Approach for Predicting Production Characteristics with Uncertainties, *Energy Conversion and Management*. (2006).

Hirschfelder, J.O., Curtiss, C.F., and Bird, R.B.: Molecular Theory of Gases and Liquids, John Wiley & Sons, 528–530. (1954).

Irvine, T.F. and Liley, P.E.: Appendix V - Thermodynamic Property Equations for Air, *Steam and Gas Tables with Computer Equations*. Academic Press, pp. 97–98. (1984).

Miller, C.W.: Wellbore User's Manual. California. (1980).

Mubarok, M.H. and Zarrouk, S.J: Discharge Stimulation of Geothermal Wells: Overview and Analysis, *Geothermics* **70**. (2017).

Pan, L., Oldenburg, C.M., Wu, Y.S. and Pruess, K.: T2Well/ECO2N Version1.0: Multiphase and Non-Isothermal Model for Coupled Wellbore-Reservoir Flow of Carbon Dioxide and Variable Salinity Water, Technical report, Lawrence Berkeley National Laboratory. (2011).

Pan, L., Oldenburg, C.M., Freifeld, B., Doughty, C., Zakem, S., Sheu, M., Cutright, B. and Terrall, T.: Fully Coupled Wellbore-Reservoir Modeling of Geothermal Heat Extraction Using CO_2 as the Working Fluid, *Geothermics* **53**, 100-113. (2015).

Tonkin, R. O'Sullivan, J. and O'Sullivan, M.: Development of a Transient, Multi-Feed Geothermal Wellbore Simulator. *Proc. 42nd New Zealand Geothermal Workshop*, Waitangi, NZ. (2020).

Ramey, H.J.: Wellbore Heat Transmission, *Journal of Petroleum Technology* **14**(04), 427–435. (1962).

Shi, H., Holmes, J.A., Durlofsky, L.J., Aziz, K., Diaz, L.R., Alkaya, B. and Oddie, G.: Drift-Flux Modeling of Two-Phase Flow in Wellbores, *SPE Journal* **10**(01), 24–33. (2005).

Vasini, E.M., Battistelli, A., Berry, P., Bonduà, S., Bortolotti, V., Cormio, C. and Pan, L.: Interpretation of Production Tests in Geothermal Wells with T2Well-EWASG, *Geothermics* **73**, 158–167. (2018).

ISSN 2703-4275